NASA/TM—2005-213867

Demonstration of Attitude Control and Bus Regulation With Flywheels

Peter E. Kascak and Ralph Jansen
University of Toledo, Toledo, Ohio

Barbara Kenny
Glenn Research Center, Cleveland, Ohio

Timothy Dever
QSS Group, Inc., Cleveland, Ohio

September 2005

The NASA STI Program Office . . . in Profile

Since its founding, NASA has been dedicated to the advancement of aeronautics and space science. The NASA Scientific and Technical Information (STI) Program Office plays a key part in helping NASA maintain this important role.

The NASA STI Program Office is operated by Langley Research Center, the Lead Center for NASA's scientific and technical information. The NASA STI Program Office provides access to the NASA STI Database, the largest collection of aeronautical and space science STI in the world. The Program Office is also NASA's institutional mechanism for disseminating the results of its research and development activities. These results are published by NASA in the NASA STI Report Series, which includes the following report types:

- TECHNICAL PUBLICATION. Reports of completed research or a major significant phase of research that present the results of NASA programs and include extensive data or theoretical analysis. Includes compilations of significant scientific and technical data and information deemed to be of continuing reference value. NASA's counterpart of peer-reviewed formal professional papers but has less stringent limitations on manuscript length and extent of graphic presentations.

- TECHNICAL MEMORANDUM. Scientific and technical findings that are preliminary or of specialized interest, e.g., quick release reports, working papers, and bibliographies that contain minimal annotation. Does not contain extensive analysis.

- CONTRACTOR REPORT. Scientific and technical findings by NASA-sponsored contractors and grantees.

- CONFERENCE PUBLICATION. Collected papers from scientific and technical conferences, symposia, seminars, or other meetings sponsored or cosponsored by NASA.

- SPECIAL PUBLICATION. Scientific, technical, or historical information from NASA programs, projects, and missions, often concerned with subjects having substantial public interest.

- TECHNICAL TRANSLATION. English-language translations of foreign scientific and technical material pertinent to NASA's mission.

Specialized services that complement the STI Program Office's diverse offerings include creating custom thesauri, building customized databases, organizing and publishing research results . . . even providing videos.

For more information about the NASA STI Program Office, see the following:

- Access the NASA STI Program Home Page at ***http://www.sti.nasa.gov***

- E-mail your question via the Internet to help@sti.nasa.gov

- Fax your question to the NASA Access Help Desk at 301–621–0134

- Telephone the NASA Access Help Desk at 301–621–0390

- Write to:
  NASA Access Help Desk
  NASA Center for AeroSpace Information
  7121 Standard Drive
  Hanover, MD 21076

NASA/TM—2005-213867

Demonstration of Attitude Control and Bus Regulation With Flywheels

Peter E. Kascak and Ralph Jansen
University of Toledo, Toledo, Ohio

Barbara Kenny
Glenn Research Center, Cleveland, Ohio

Timothy Dever
QSS Group, Inc., Cleveland, Ohio

Prepared for the
39th Annual Meeting
sponsored by the Institute of Electrical and Electronics Engineers
Industry Applications Society
Seattle, Washington, October 3–7, 2004

National Aeronautics and
Space Administration

Glenn Research Center

September 2005

Available from

NASA Center for Aerospace Information
7121 Standard Drive
Hanover, MD 21076

National Technical Information Service
5285 Port Royal Road
Springfield, VA 22100

Available electronically at http://gltrs.grc.nasa.gov

Demonstration of Attitude Control and Bus Regulation with Flywheels

Peter Kascak and Ralph Jansen
University of Toledo
Toledo, Ohio 43606

Barbara Kenny
National Aeronautics and Space Administration
Glenn Research Center
Cleveland, Ohio 44135

Timothy Dever
QSS Group Inc.
Cleveland, Ohio 44135

Abstract

A flywheel energy storage device stores energy in a rotating mass. These devices can be used to perform the same function as traditional chemical batteries. In terms of the energy storage function, a flywheel system has significant advantages over chemical batteries: length of life, energy density, power density, and the capability of deep depth of discharge. Also, flywheels can be used to control the attitude of the spacecraft. This paper describes an experiment using two flywheels to simultaneously regulate a DC bus and provide single axis angle regulation on an air table. Models of the mechanical and electrical systems are developed, and simulations are run, then compared to experimental results. The correspondence of the simulations and experiments shows the sufficiency of the modeling of subsystems.

I. Introduction

Flywheel energy storage is an ongoing research activity at NASA Glenn Research Center. The concept is to replace chemical batteries on spacecraft with devices that store their energy mechanically, in a spinning disk. Power is delivered and taken from the flywheel with a motor/generator. The flywheel is magnetically levitated to reduce drag and increase life. The advantages of flywheel energy storage over chemical batteries are energy density, lifetime, and the ability to provide spacecraft attitude control. Full three axis spacecraft attitude control and energy storage can be obtained with 4 flywheels, with the flywheels arranged in tetrahedral shape.

This paper describes a single axis attitude control and bus regulation experiment, using two flywheels on a low friction air table. Although the concept of using flywheel energy storage units for attitude control is well documented in the literature (refs. 1 to 4), the literature does not describe motor control or bus regulation. This experiment is the first working prototype bus and angle regulation test. A motor control algorithm to regulate the bus and attitude was developed by NASA Glenn Research Center (GRC) (ref. 5), and testing of torque developed in a two flywheel system with a stationary air table restrained by load cells was conducted at GRC (ref. 6). This paper describes an experiment which uses the control algorithm in (ref. 5) to demonstrate bus voltage regulation and single axis attitude (angle) control on an unrestrained air table. Models of the electrical and mechanical systems are developed, and simulations are run, then compared to experimental results.

II. Test Setup

In this experiment, two technology demonstrator flywheel modules developed under two different flight programs were integrated at NASA GRC's High Energy Flywheel Facility (HEFF). Figure 1 shows this facility, which includes an air table where the flywheel modules are mounted. The cardboard boxes surrounding the flywheels are filled with water bottles and provide a safety containment system (ref. 7). Surrounding the water filled boxes is a Kevlar shroud. Thermal, vacuum, and instrumentation support hardware can be seen on the upper platform. A simple schematic of the setup is shown in figure 2. This hardware setup is used for the demonstration of a flywheel system which provides simultaneous power bus regulation and single axis torque and attitude (table angle) control.

III. Mechanical System

The flywheel modules which are incorporated into HEFF are called D1 and HSS. The mechanical plant models included in the system are the D1 flywheel module, the HSS flywheel module, and the single degree of freedom plant model.

The D1 Flywheel Module (D1) and the High Speed Shaft (HSS) flywheel module used in this test are not identical, however they both have generally the same topology. They each have magnetically suspended rotors with permanent magnet motor/generators, mechanical touchdown bearings, and an integral housing/vacuum enclosure. Table 1 contains the flywheel module properties.

TABLE 1.—SYSTEM PROPERTIES

	Value	Property
System		
J_0	15 kg·m^2	platform inertia about axis 0
c	.5 kg·m^2·s^{-1}	platform damping
k	1 kg·m^2·s^{-2}	platform stiffness
D1 Flywheel Module		
m_{r1}	17.2 kg	rotor mass
J_{r1}	0.0664 kg·m^2	rotor polar moment of inertia
m_{s1}	61.2 kg	stator mass
J_{s1}	560 kg·m^2	stator polar moment of inertia
x_1	0.254 m	distance from axis 0 to 1
L_{q1}	0.000025 H	q axis inductance of motor
L_{d1}	0 .000019 H	d axis inductance of motor
R_{s1}	0.0145 Ω	l-n stator resistance of motor
λ_{af1}	0.00733 V-s	rotor magnet flux linkage
B_1	0	viscous drag on rotor
HSS Flywheel Module		
m_{r2}	6.53kg	rotor mass
J_{r2}	0.00377 kg·m^2	rotor polar moment of inertia
m_{s2}	56.7 kg	stator mass
J_{s2}	518 kg·m^2	stator polar moment of inertia
x_2	0.254 m	distance from axis 0 to 2
L_{q2}	0.000142 H	q axis inductance of motor
L_{q2}	0.000101 H	d axis inductance of motor
R_{s2}	0.035 Ω	l-n stator resistance of motor
λ_{af2}	0.014456 V-s	rotor magnet flux linkage
B_2	0	viscous drag on rotor
Base		
m_b	40.1kg	base mass
J_b	2939 kg·m^2	base polar moment of inertia
Avionics		
m_a	40.1kg	avionics mass
J_a	2939 kg·m^2	avionics polar moment of inertia
C	5860 μF	dc bus capacitance

The mechanical system is modeled as a single degree of freedom, second order system. The air table and all the components mounted on it, other than the flywheel rotors, will be referred to as the platform. The platform components are modeled as inertias about the spin axis of air table. These components are the base, avionics, and flywheel stator assemblies. The flywheel rotors are included as torques acting on the platform. Figure 3 shows a free body diagram of the system. Axes 0, 1, and 2 represent the rotation axes of the platform, flywheel 1, and flywheel 2 respectively. The equation of motion for the platform is:

Figure 1.— High Energy Flywheel Facility (HEFF).

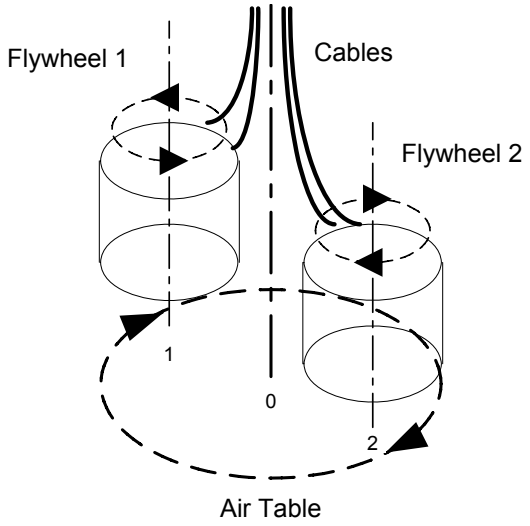

Figure 2.—HEFF schematic.

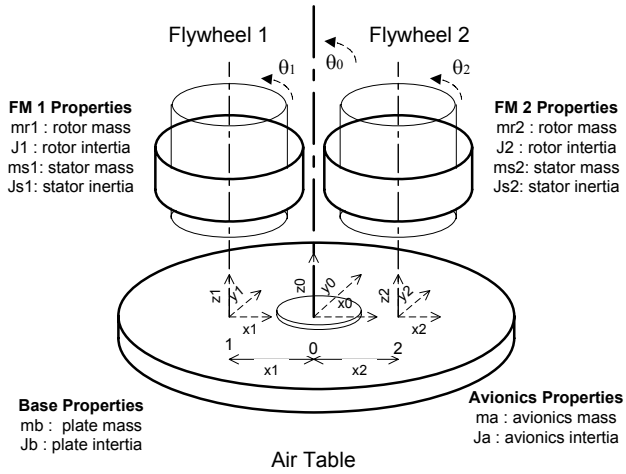

Figure 3.—Free body diagram.

$$J\ddot{\theta}_0 + c\dot{\theta}_0 + k\theta_0 = \sum T \quad (1)$$

The total inertia about the 0 axis, J_0, is the sum of the inertias of the base (J_b), avionics (J_a), flywheel stator assemblies (J_{s1} and J_{s2}), and flywheel rotors (J_{r1} and J_{r2}). The base and avionics are modeled as circular cylinders, the flywheel stators are considered circular cylindrical shells located on a parallel axis, and the flywheel rotors are modeled as circular cylinders on parallel axis. Using standard equations (ref. 8) the total inertia about the 0 axis is

$$\begin{aligned} J_0 = {} & J_a + J_b + \\ & (J_{r1} + m_{r1}x_1^2) + (J_{s1} + m_{s1}x_1^2) \\ & (J_{r2} + m_{r2}x_2^2) + (J_{s2} + m_{s2}x_2^2) \end{aligned} \quad (2)$$

The flywheel module is modeled as a single degree of freedom rotor with a torque applied by the motor/generator, and the motor is modeled as a synchronous permanent magnet machine (ref. 9). The torques applied to the platform are equal and opposite to the torque applied to the rotors of each flywheel model. Since rotor translation velocity is assumed to be slow and gyroscopic forces are neglected, the platform inertia reacts to the sum of the torques (ref. 5) according to

$$\sum T = T_p = -T_{e1} - T_{e2} \quad (3)$$

IV. Electrical System model

The model of the electrical system used in this experiment includes: the DC bus plant model, the power supply plant model, and the load plant model. Each of these models is described in the following paragraphs.

The DC bus is modeled as a capacitor with various current sources charging or discharging it (fig. 4). These currents are the inputs to the DC bus model and consist of: the DC currents supplying the flywheels (I_{DC1} + I_{DC2}), the power supply current ($I_{P/S}$), and the load current (I_{load}).

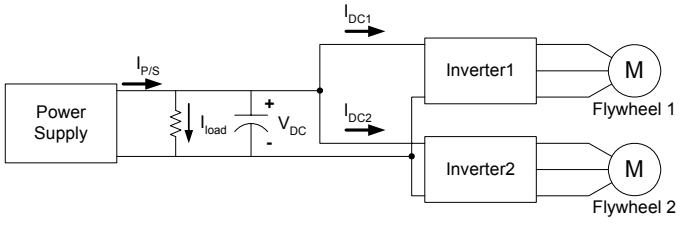

Figure 4.—Electrical system schematic.

The power supply is modeled as a voltage regulating current source. The power supply model has two inputs, one for a voltage set point and one for a current limit. The power supply will provide whatever current, $I_{P/S}$, is necessary to keep the bus voltage at the voltage set point as long as the current is less than the current limit. To accomplish this in the model, the error between the voltage set point and the bus voltage is taken. This error is run through a PI control law to provide a current command. This current command is compared to the current limit. If the command is less than the current limit, $I_{P/S}$ is equal to the current command. If the current command is greater than the current limit, $I_{P/S}$ is equal to the current limit.

The load is modeled as a resistor. Thus the current consumed by the load is just the DC bus voltage divided by the value of the resistor.

V. DC Bus and Attitude Controller

The DC bus and attitude controller includes: a current regulator for each flywheel, a DC bus regulator, an attitude regulator, and an inertia and DC bus coordinator (IDCBC). The IDCBC is the heart of the DC bus and attitude controller, and it has five inputs. The two key inputs are passed from the DC bus regulator (total DC current command, I_{DC}* - in this paper, command signals are designated with a '*') and the attitude regulator (total torque command, Torque*). The remaining three inputs are also crucial, but are relatively static compared to I_{DC}* and Torque*; they are the DC bus voltage (V_{DC} or V_{DC}*) and the flywheels' angular velocities (ω_{r1} and ω_{r2}). The IDCBC uses the key inputs (I_{DC}* and Torque*) to calculate the flywheel motor-generator rotational reference frame q-axis current commands required to provide simultaneous control of the DC bus and table angle, i^{*r}_{qs1} and i^{*r}_{qs2}. These commands are then fed to the appropriate flywheel motor current regulators.

The two motors are controlled by a sensorless field orientation algorithm. The d-axis rotational reference frame current is commanded to zero and the q-axis rotational reference frame current command varies to provide attitude control and bus regulation. A general description of field orientation of permanent magnet machines can be found in (ref. 9) and a specific discussion of the motor control techniques used in the flywheel program can be found in (refs. 10 and 11).

The DC bus on a low earth orbit spacecraft, such as the International Space Station, operates in one of three DC bus regulation modes: charge mode, charge reduction mode, and discharge mode. The proper operating mode is selected and controlled by the DC bus regulator portion of the DC bus and attitude controller; each operating mode is described in detail in the following paragraphs.

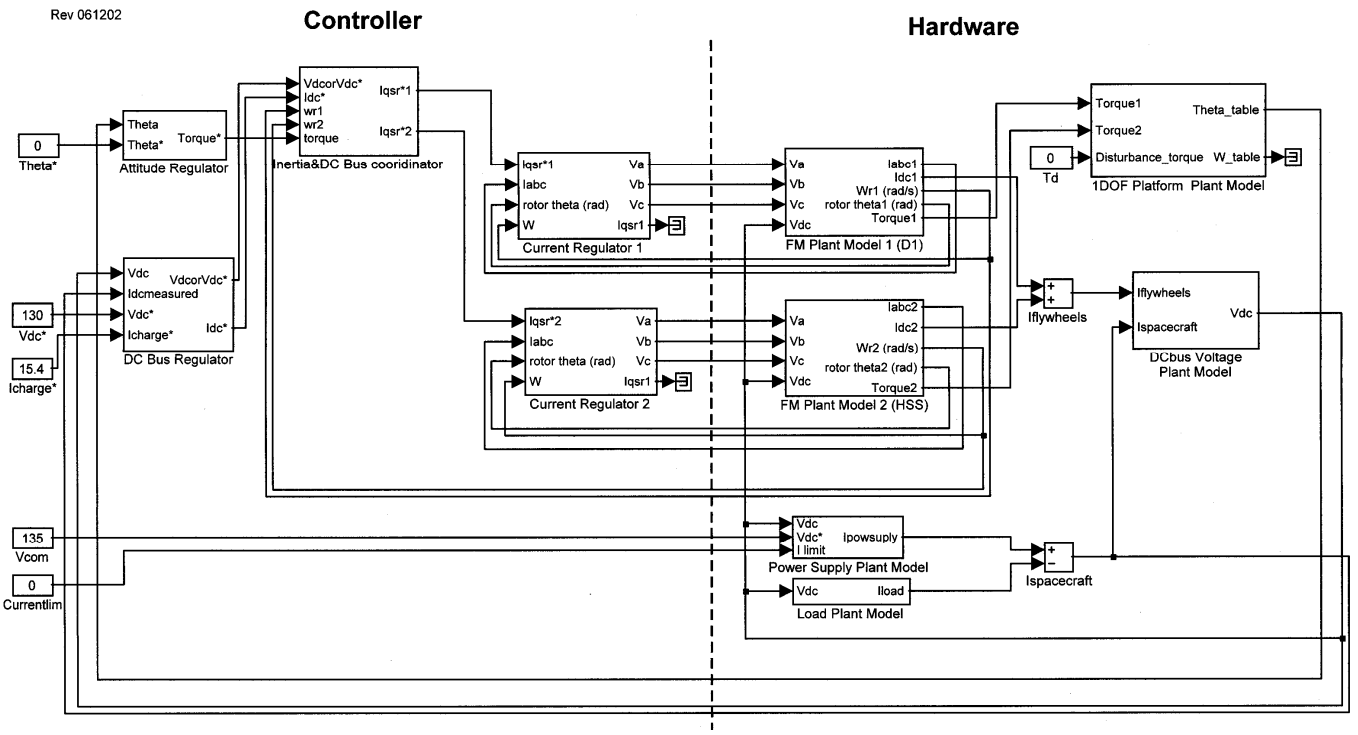

Figure 5.—System model of DC bus and attitude controller and hardware.

The DC bus on a low earth orbit spacecraft, such as the International Space Station, operates in one of three DC bus regulation modes: charge mode, charge reduction mode, and discharge mode. The proper operating mode is selected and controlled by the DC bus regulator portion of the DC bus and attitude controller; each operating mode is described in detail in the following paragraphs.

The charge mode represents operation in full sun, when the photovoltaics system provides current and voltage regulation. In the charge mode, the DC bus regulator charges the flywheel system at a charge current set point (I^*_{charge}).

The charge reduction mode represents operation in partial sun when the current generated by the photovoltaics system is not sufficient to meet both the load demand and the flywheel charge set point. During charge reduction mode, the flywheel system regulates the DC bus voltage to V^*_{dc}.

The discharge mode represents operation in eclipse when the photovoltaics system provides less current than required by the load, and the flywheel system provides the remaining required load current. As in charge reduction mode, the flywheel system regulates the DC bus voltage to V^*_{dc}.

In both charge reduction mode and discharge mode the DC bus regulation algorithm uses the DC current from each of the two flywheel inverters to regulate the bus voltage. More detail on the DC bus regulator and the modes of operation can be found in (refs. 12 to 14).

The desired table torque, T_P, is generated by the attitude regulator. The attitude regulator is a PID controller, with table angular position and commanded angle position as inputs.

The IDCBC converts the desired table torque T_P and DC current I_{DC} into the q-axis rotational reference frame current commands to the two flywheel motor controllers, i^{*r}_{qs1} and i^{*r}_{qs2} which provide both attitude control and DC bus regulation. The first relationship necessary to determine the appropriate current commands defines I_{DC} as a function of i^{*r}_{qs1} and i^{*r}_{qs2}, and starts with the power balance. The AC power in one of the flywheel motors can be expressed as shown in (ref. 15).

$$P_{flywheel} = \frac{3}{2}(v^r_{qs} i^r_{qs} + v^r_{ds} i^r_{ds}) \tag{4}$$

Since the d-axis current is regulated to zero, and neglecting losses so that we can equate AC and DC power, the following expression is obtained, where $I_{DC,m}$ is the DC current into one of the flywheel motor inverters:

$$V_{DC} I_{DC,m} = \frac{3}{2}(v^r_{qs} i^r_{qs}) \tag{5}$$

The q-axis voltage equation, from (ref. 9), is:

$$v^r_{qs} = i^r_{qs} R_s + L_{qs} p i^r_{qs} + i^r_{ds} \omega_r L_{ds} + \omega_r \lambda_{af} \tag{6}$$

In steady state the derivative term goes to zero; since the d-axis current is regulated to zero and the resistive term is much smaller than the back emf term (especially at high speeds), we have, from (ref. 12),

$$V_{DC} I_{DC,m} \approx \frac{3}{2}(\omega_r \lambda_{af} i^r_{qs}) \tag{7}$$

Rearranging (7), we get an expression for the DC current $I_{DC,m}$ in terms of the rotational reference frame q-axis current, i^r_{qs}, with a dependence on a the rotor flux linkage, λ_{af}, the rotor speed, ω_r, and the DC bus voltage V_{DC}.

$$I_{DC,m} \approx \frac{3\omega_r \lambda_{af}}{2V_{DC}} i^r_{qs} \tag{8}$$

The total DC bus current, I_{DC}, is the sum of the two motor inverter DC currents, I_{DC1} and I_{DC2}., as seen in figure 4. Considering this, equation (8) can be used to meet the goal of expressing I_{DC} as a function of i^{*r}_{qs1} and i^{*r}_{qs2}:

$$I_{DC} = c i^r_{qs1} + d i^r_{qs2} \tag{9}$$

where

$$c = \frac{3\omega_{r1}\lambda_{af1}}{2V_{DC}} \tag{10}$$

and

$$d = \frac{3\omega_{r2}\lambda_{af2}}{2V_{DC}} \tag{11}$$

Next, we would like an expression for the total torque applied to the platform as a function of i^{*r}_{qs1} and i^{*r}_{qs2}. The torque applied to the platform by each flywheel is equal and opposite to the torque applied to its rotor by that flywheel's motor-generator. The expression for torque produced by the flywheel PM motor-generator is given as (ref. 9)

$$T_e = \frac{3}{2}\frac{P}{2}\left[\lambda_{af} + \left(L_d - L_q\right) i^r_{ds}\right] i^r_{qs} \tag{12}$$

where P is the number of poles in the motor-generator. Since the rotational reference frame d-axis current is controlled to be zero, this torque can be expressed as:

$$T_e = \frac{3}{2}\frac{P}{2}\lambda_{af} i^r_{qs} \tag{13}$$

The total torque that is applied to the platform is the negative sum of the two motor torques, T_{e1} and T_{e2}. Using equations (3) and (13), this relationship can be used to meet the goal of expressing total platform torque, T_P, as a function of i^{*r}_{qs1} and i^{*r}_{qs2}:

$$T_p = -T_{e1} - T_{e2} = -a i^r_{qs1} - b i^r_{qs2} \tag{14}$$

where

$$a = \frac{3}{2}\frac{P_1}{2}\lambda_{af1} \tag{15}$$

and

$$b = \frac{3}{2}\frac{P_2}{2}\lambda_{af2} \tag{16}$$

By solving equations (9) and (14) simultaneously, the control variables i^r_{qs1} and i^r_{qs2} can be found in terms of desired DC bus current, I_{DC}, and the platform torque, T_p. The result is given in equations (17) and (18).

$$i^r_{qs1} = \frac{bI_{DC} + dT_p}{cb - da} \tag{17}$$

$$i^r_{qs2} = \frac{T_p + a i^r_{qs1}}{-b} \tag{18}$$

VI. Simulation Results

In order to simulate the experiment, the models for the mechanical system, electrical system and the DC bus and attitude controller were built up and integrated. The HSS and D1 were modeled in the system, incorporating the system parameters defined in table 1.

A set of simulations, testing relevant system performance, were picked to mimic experimental runs in the HEFF facility. Details of each simulation are presented in table 2. They include table angle steps in both charge and discharge modes (runs 1 and 4), commanded current step in charge mode (run 2), and load step change in discharge mode (run 3).

TABLE 2.—SIMULATION CONDITIONS

Simulation Run	Test	Mode	Figures
1	Angle step	Charge	6-9
2	I*charge step	Charge	10-11
3	Load step	Discharge	12-15
4	Angle step	Discharge	16-18

Simulations of the system were run at 59 kRPM; this represents the maximum design speed of the flywheel units under test.

Simulation run 1 simulates a commanded angle step in charge mode. Under this test condition, both flywheels are charging, the bus is regulated by the DC supply, and the flywheel speeds must change in order to apply the table torque necessary to change table angle. The results of run 1 are presented in figures 6 to 9.

Figure 6 shows the angle response to the step change. Note that the response is underdamped; this tuning was chosen to

provide a relatively fast response. Less ringing could be achieved by increasing derivative damping, if desired.

Figure 7 shows the speed changes of the two flywheels which provide the desired angle step change. Note that HSS acceleration is much greater than D1; this is as expected, since the HSS rotor has considerably lower inertia than the D1 rotor.

Figure 8 shows the DC bus voltage during a charge step. The bus voltage remains flat, as expected; this run condition mimics a DC power supply run well under its current limit.

Figure 9 shows the DC currents of the individual flywheels, as well as the DC bus current, during the angle step. Note that although the individual flywheel DC currents vary in order to provide the required torque, the sum of the two flywheel currents is constant, adding up to the total commanded DC bus current I_{DC}*, as required.

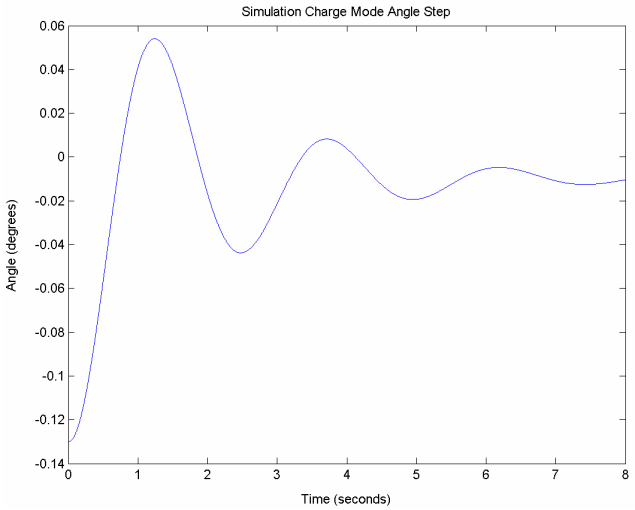

Figure 6.—Simulated angle step in charge mode: angle.

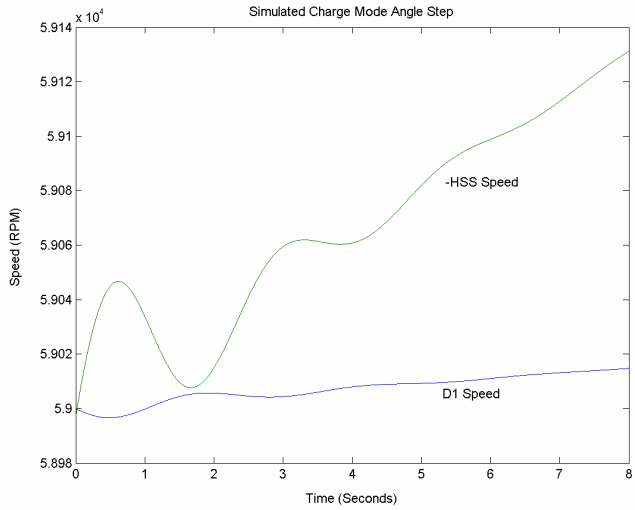

Figure 7.—Simulated angle step in charge mode: speed.

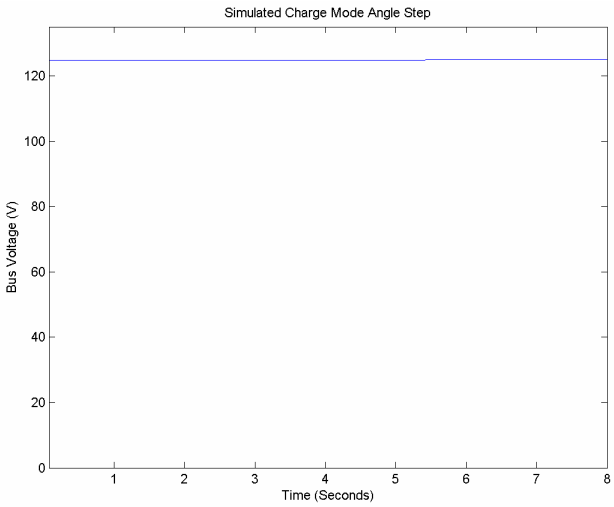

Figure 8.—Simulated angle step in charge: voltage.

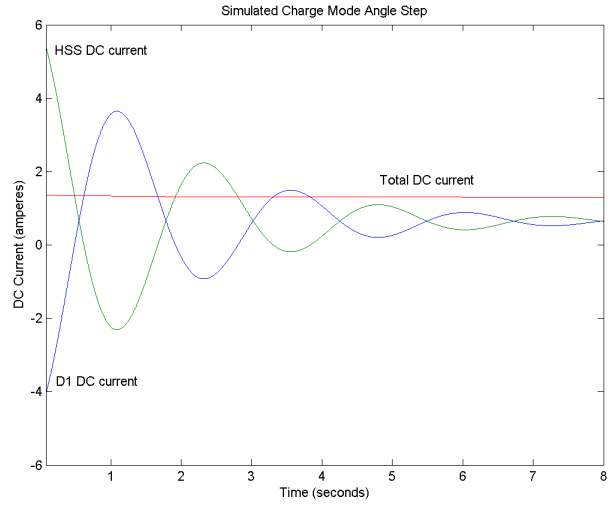

Figure 9.—Simulated angle step in charge: bus current.

Simulation run 2 simulates a commanded current step in charge mode. Under this test condition, both flywheels again are charging and the bus is regulated by the DC supply, and the flywheel speeds must change in order to accept more DC bus current, while maintaining table torque (and thus table angle). The results of run 2, are presented in figures 10 and 11.

Figure 10 shows the simulated current step. Note that the individual flywheel currents add up to the total current command, as required.

Under these conditions, table torque must be controlled to zero in order to maintain table angle. Figure 11 shows the disturbance on the angle by the charge current set point step; the disturbance in the angle is very minor, as desired. This demonstrates good decoupling between the DC bus regulator and the attitude regulator.

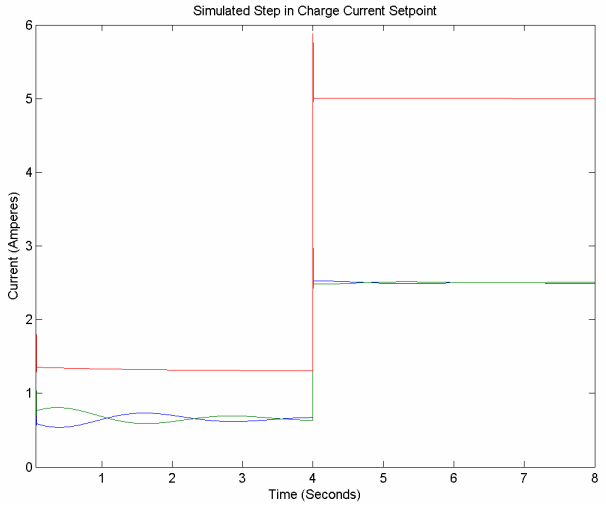

Figure 10.—Simulated step in charge current.

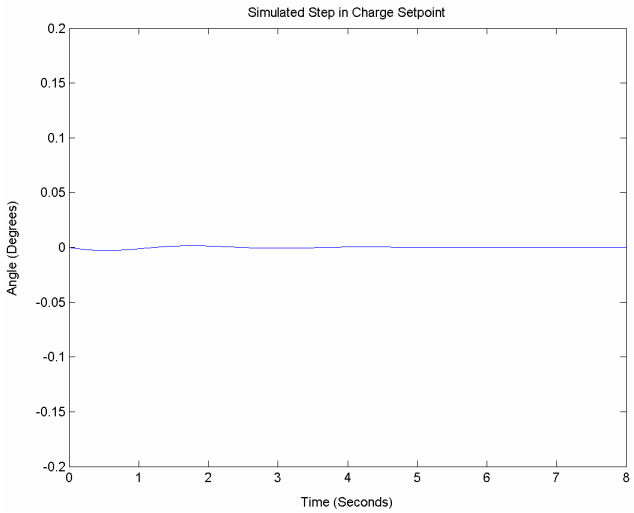

Figure 11.—Simulated angle response to charge current step.

Simulation run 3 simulates a load step change in discharge mode. Under this test condition, both flywheels are discharging, and the flywheel speeds must change in order to provide additional current while regulating bus voltage and table angle. The results of run 3 are presented in figures 12 to 15.

Figure 12 shows the bus voltage during this load step change. Note that, as desired, bus voltage is held very well.

Figure 13 shows the bus current during this load step. Note that the sign of the currents is negative, implying that the flywheels are supplying current, and that the sum of the two flywheel currents adds up to the total current change, as required.

Figure 14 shows the angle disturbance caused by the load step; note that, as desired, the angle disturbance is minor.

Figure 15 shows the speed response during load step. As expected, HSS speed change is greater than D1, due to the lower inertia of the HSS rotor.

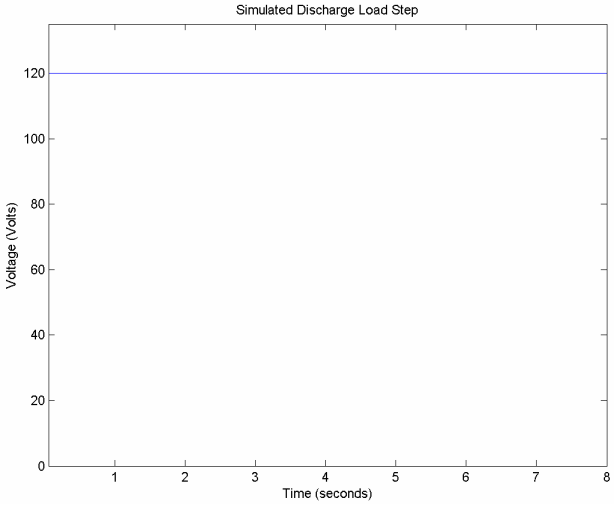

Figure 12.—Simulated load step in discharge mode: voltage.

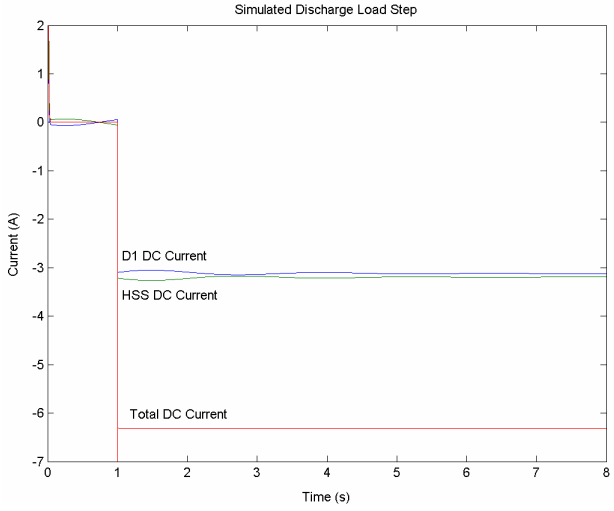

Figure 13.—Simulated load step in discharge mode: current.

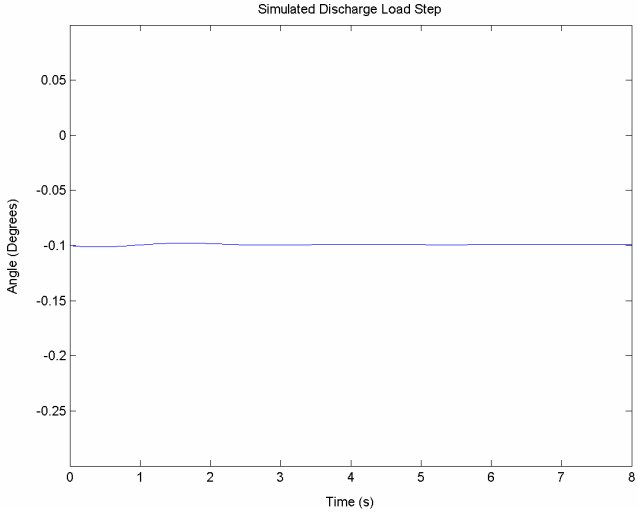

Figure 14.—Simulated load step in discharge mode: angle.

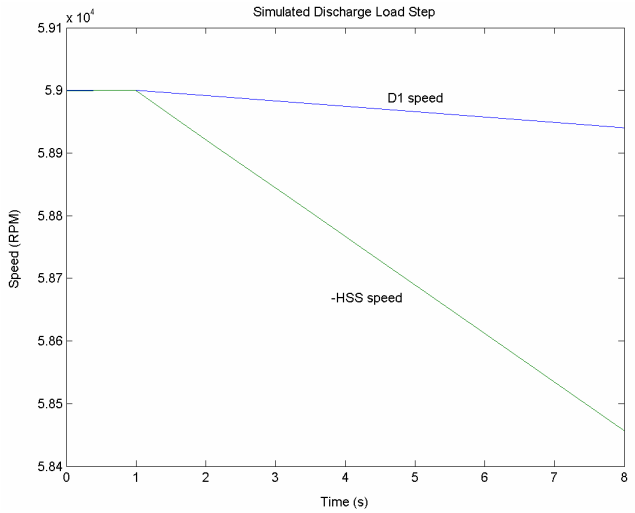

Figure 15.—Simulated load step in discharge mode: speed.

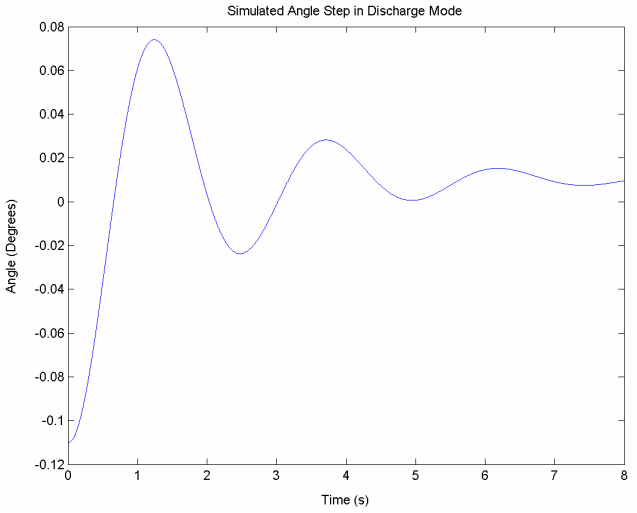

Figure 16.—Simulated angle step in discharge mode: angle.

Simulation run 4 simulates an angle step change in discharge mode. Under this test condition, both flywheels are discharging, and the flywheel speeds must change in order to provide a table angle change while maintaining the sum of the flywheel currents and regulating the bus voltage. The results of simulation run 4 are presented in figures 16 to 18.

Figure 16 shows the angle response to the step change in angle command. Once again, the response is underdamped, and the step change matches the command value.

Figure 17 shows the DC currents of the individual flywheels, as well as the DC bus current, during the angle step. Note that although the individual flywheel DC currents vary in order to provide the required torque, the sum of the two flywheel currents is constant, adding up to the total commanded DC bus current I_{DC}*, as required.

TABLE 3. EXPERIMENTAL`—TEST CONDITIONS.

Experimental Run	Test	Mode	Figures
1	Angle step	Charge	19-22
2	I*charge step	Charge	23-24
3	Load step	Discharge	25-28
4	Angle step	Discharge	29-31

Figure18 shows the bus voltage during this disturbance. There is no appreciable disturbance on the DC bus voltage caused by the angle step, as desired.

VII. Experimental Results

Experiments testing combined bus regulation and single axis attitude control were run on the HSS and D1 flywheels, mounted on the low friction air table, in the HEFF facility. Details on the experimental runs, which were selected to test the relevant system performance, are presented in table 3.

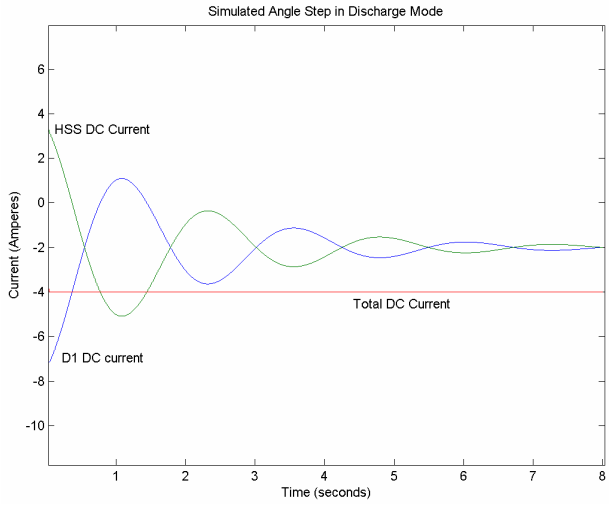

Figure 17.—simulated angle step in discharge mode: current.

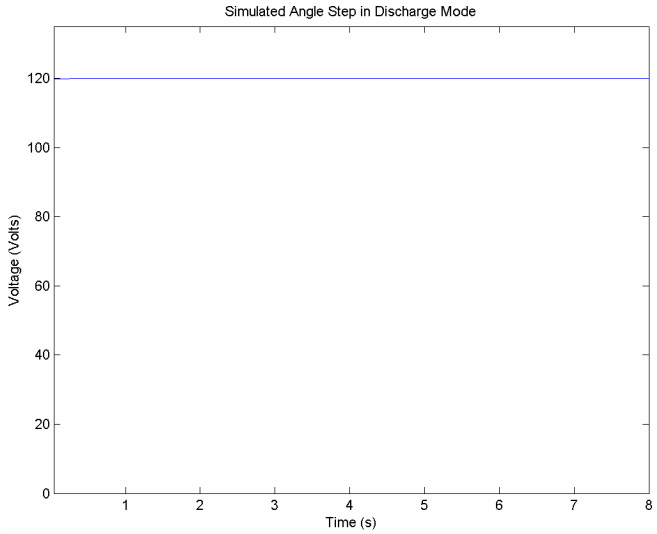

Figure 18.—simulated angle step in discharge mode: voltage.

They include table angle steps in both charge and discharge modes (runs 1 and 4), commanded current step in charge mode (run 2), and load step change in discharge mode (run 3). Experimental runs were performed at the low end of the flywheel operating range, between 8 and 20 kRPM; this speed range was selected because the HSS is limited by the bus voltage to 22 kRPM.

Note that the experimental runs mirror the simulation runs; results from the tests in the HEFF facility will be compared below to the results of the modeling run counterparts.

Experimental run 1 demonstrates a commanded angle step in charge mode. As in simulation run 1, in this test case both flywheels are charging, the bus is regulated by the DC supply, and the flywheel speeds must change in order to apply the table torque necessary to change table angle. The results of experimental run 1 are presented in figures19 to 22.

Figure 19 shows the angle response to the step change. The angle step size of ~0.1 degree was chosen because it is the largest angle step achievable given the present hardware configuration (low flywheel speed and the low moment of inertia of the HSS rotor). Achievable steps of this small size in hardware demonstrate the fine resolution of the attitude controller.

As can be seen in figure 19, the response rings at about 0.35 Hz; this frequency is determined by the torsional spring constant of the HEFF cabling, and the rotational inertia of the table. The dynamic response of these tests was used to determine the platform damping and stiffness of the model (c and k, table 1). Note that the test response is similar to the modeled response, although the model damps out more quickly. The mismatch in damping is due to the cabling which brings power to the HEFF air table. This cabling behaves like a hysteretic spring, and so the linear spring used in the model does not capture the hysteretic nature of the cabling. However, further modeling of this spring is not necessary, because, in a space application, there will be no cabling effect.

Figure 20 shows the speed changes of the two flywheels which provide the desired angle step change. Note that, before the step change, the D1 is accelerating and the HSS is decelerating. This is also due to cabling effects; the hysteresis forces the position regulator in the controller to maintain a torque on the table, even during steady state, in order to maintain the table angle. Due to this effect, the torque on the table through the step is different than that in the simulation, which causes the accelerations for the two flywheel rotors to be different. Once again, this effect is unimportant, because in a space application, neither the spring constant nor the hysteresis will exist.

Figure 21 shows the DC bus voltage during a charge step. The bus voltage is held flat, as expected, by the DC power supply in the HEFF facility.

Figure 22 shows the DC currents of the individual flywheels, as well as the DC bus current, during the angle step. Note that although the individual flywheel DC currents

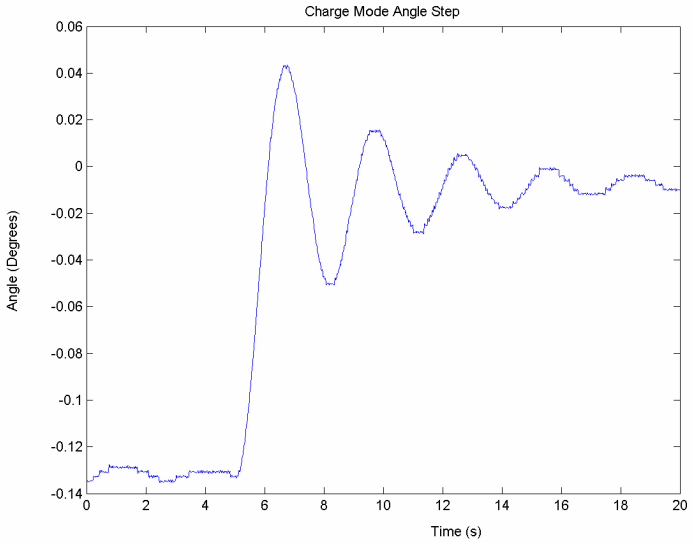

Figure 19.—Angle step in charge mode: angle.

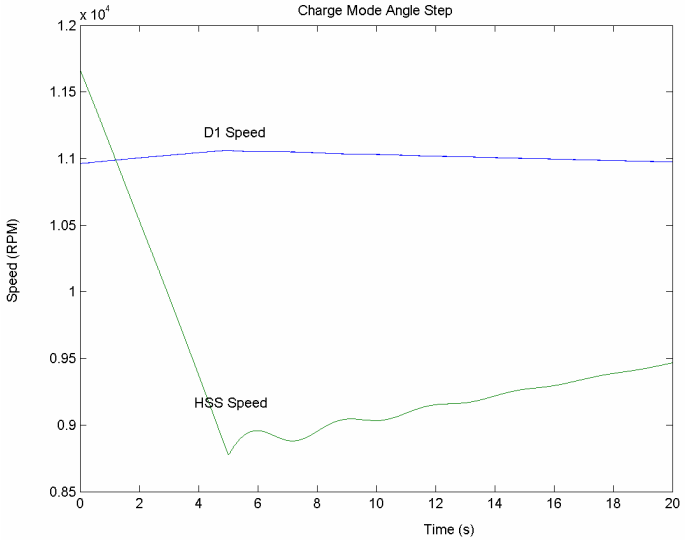

Figure 20.—Angle step in charge mode: speed.

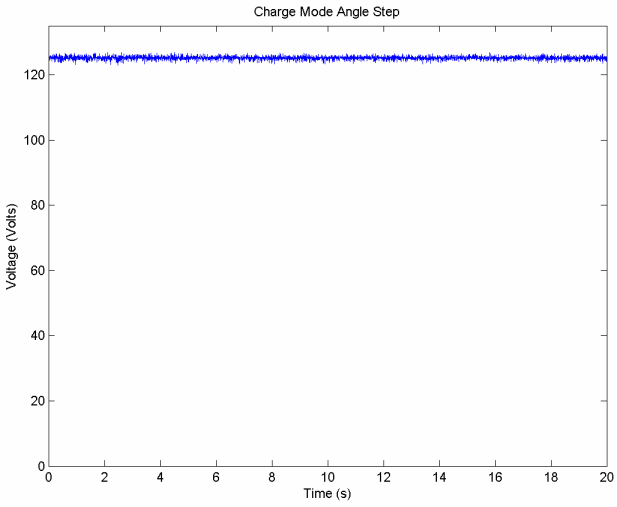

Figure 21.—Angle step in charge mode: voltage.

vary in order to provide the required torque, the sum of the two flywheel currents is constant, adding up to the total commanded DC bus current I_{DC}*, as required. This also closely mimics the simulation run 1 results.

Experimental run 2 demonstrates a commanded current step in charge mode. As in simulation run 2, both flywheels again are charging and the bus is regulated by the DC supply, and the flywheel speeds must change in order to accept more DC bus current while maintaining table torque (and thus table angle). The results of experimental run 2 are presented in figures 23 and 24.

Figure 23 shows the simulated current step. Note that the individual flywheel currents add up to the total current command, as required. This result agrees with the simulation run, except for the current divergence after about ten seconds. As seen on the figure, the HSS DC current increases with time, while the D1 current decreases. This is due the hysteretic torque of the HEFF cables, as described above; continuous torque must be applied, even in steady state, to maintain the table position. Note that the sum still adds to the total DC current, as required.

Under these conditions, table torque must be controlled to zero in order to maintain table angle. Figure 24 shows the disturbance on the angle by the charge current set point step; the disturbance in the angle is very minor, as desired. This demonstrates good decoupling between the DC bus regulator and the attitude regulator in the hardware implementation.

Experimental run 3 demonstrates a load step change in discharge mode. As in simulation run 3, both flywheels are discharging, and the flywheel speeds must change in order to provide additional current while regulating bus voltage and table angle. The results of experimental run 3 are presented in figures 25 to 28.

Figure 25 shows the bus voltage during this load step change. Note that, in hardware, the bus voltage is maintained by the flywheel system during the load step, as desired.

Figure 26 shows the bus current during this load step. Note that the sign of the currents is negative, implying that the flywheels are supplying current, and that the sum of the two flywheel currents adds up to the total current change, as required. This is similar to the simulation run, except for the DC current divergences, due to the HEFF cable hysteretic torque as described above.

Figure 27 shows the angle disturbance caused by the load step; note that, as desired, the angle disturbance is minimized in the hardware test.

Figure 28 shows the speed response during load step. Note that, as expected, the resultant HSS speed change is greater than that of D1, due to the lower inertia of the HSS rotor.

Experimental run 4 demonstrates an angle step change in discharge mode. As with simulation run 4, both flywheels are discharging, and the flywheel speeds must change in order to provide a table angle change while maintaining the sum of the flywheel currents and regulating the bus voltage. The results of experimental run 4 are presented in figures 29 to 31.

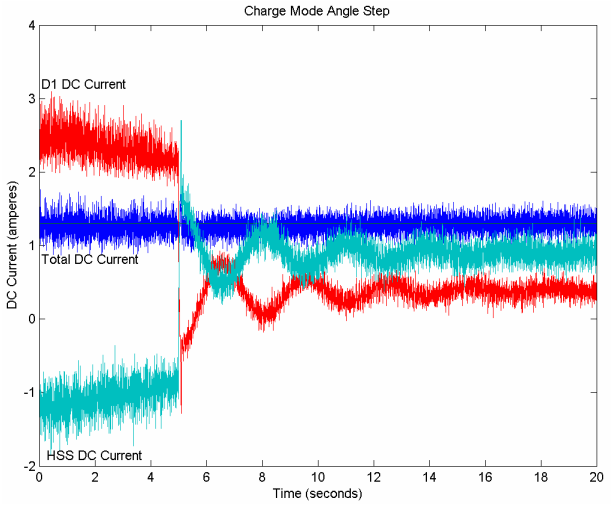

Figure 22.—Angle step in charge mode: DC current.

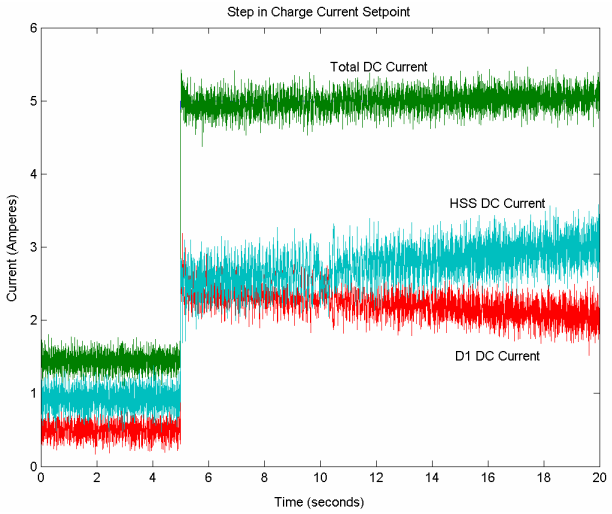

Figure 23.—Step in charge current.

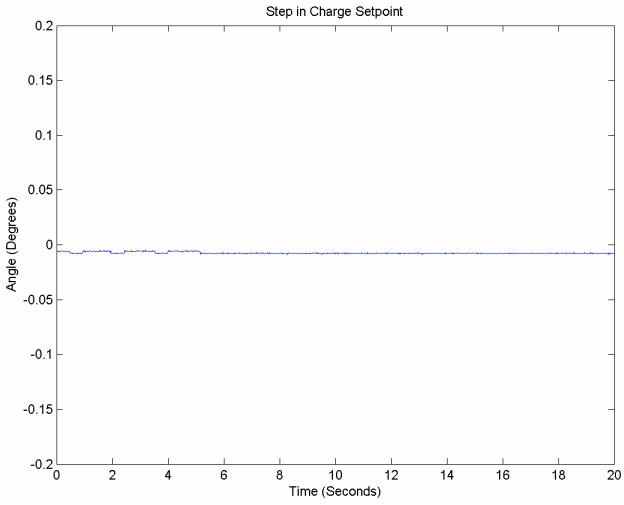

Figure 24.—Angle response to charge current step.

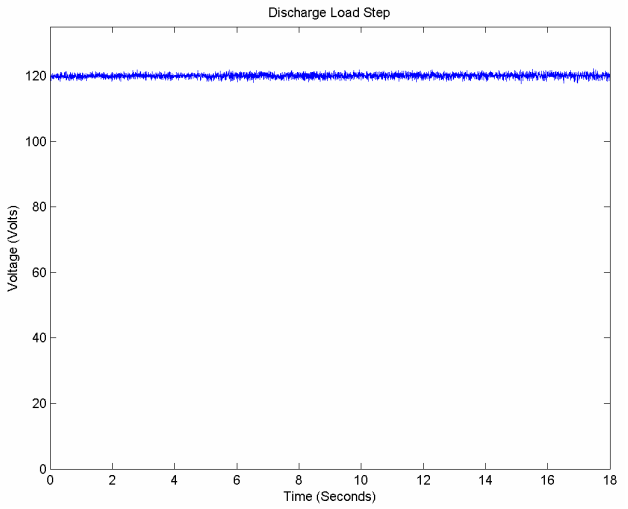

Figure 25.—Load step in discharge mode: voltage.

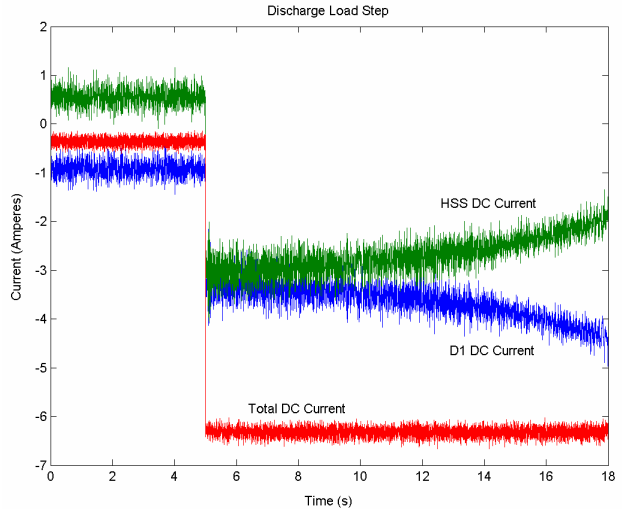

Figure 26.—Load step in discharge mode: current.

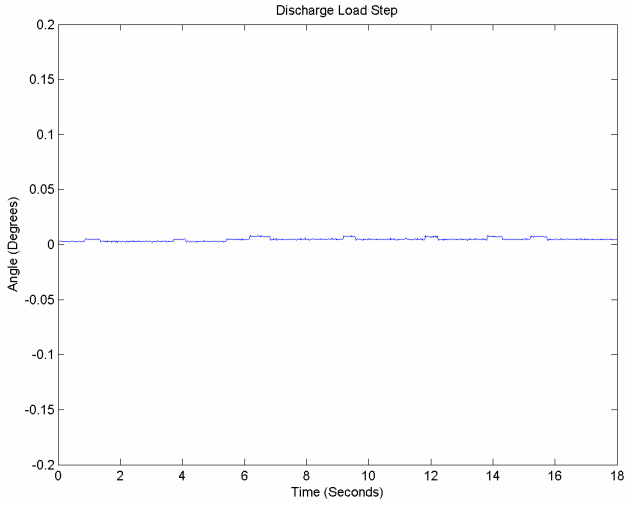

Figure 27.—Load step in discharge mode: angle.

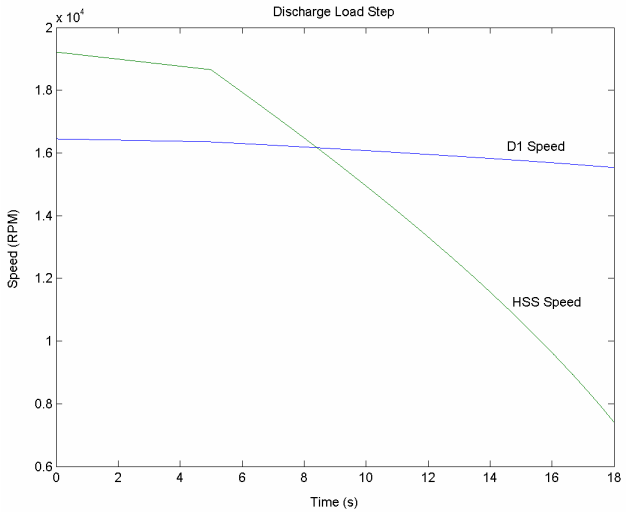

Figure 28.—Load step in discharge mode: speed.

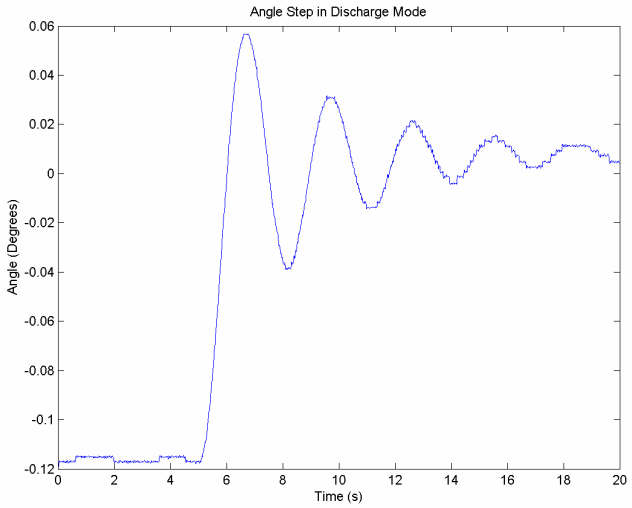

Figure 29.—Angle step in discharge.

Figure 29 shows the angle response to the step change in angle command. As with experimental run 1, which performed an angle step in charge mode, the response here is underdamped.

Figure 30 shows the DC currents of the individual flywheels, as well as the DC bus current, during the angle step. Once again, the individual flywheel DC currents vary in order to provide the required torque, the sum of the two flywheel currents is constant, adding up to the total commanded DC bus current I_{DC}*, as required.

Figure 31 shows the bus voltage during the angle change. Note that the flywheel system does effectively regulate the DC bus voltage during the angle step, as desired.

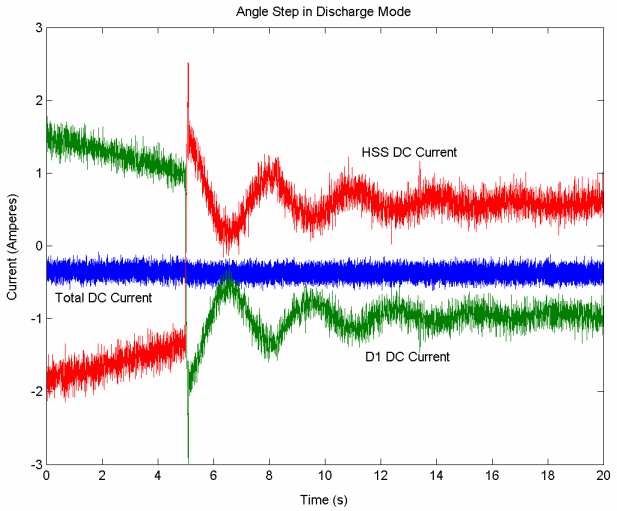

Figure 30.—Angle step in discharge: bus current.

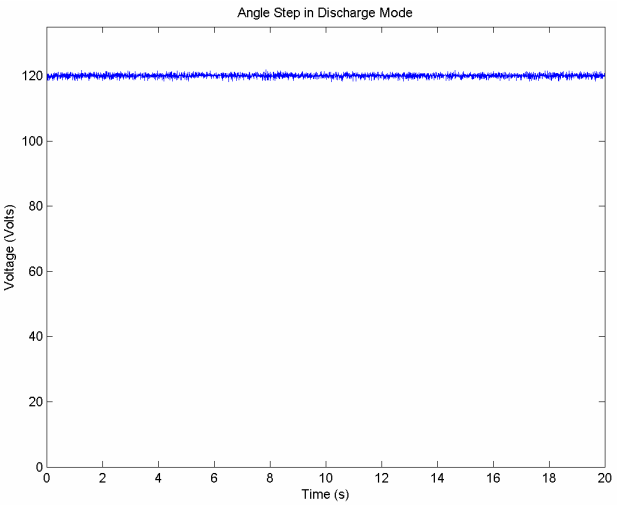

Figure 31.—Angle step in discharge: voltage.

VIII. Conclusions

This paper has presented an experiment demonstrating single axis attitude control and bus regulation. Two flywheels with different performance characteristics have been integrated onto a low friction air table in the High Energy Flywheel Facility (HEFF) at NASA Glenn Research Center in Cleveland, Ohio. In this paper, models of the electrical and mechanical systems used in the experiment are developed, and the control algorithm to allow simultaneous bus regulation and attitude control is presented. The separate models are integrated with the control algorithm to allow simulation of the system.

Four different test runs, which exercise the relevant control modes, are presented. Each of these test cases is run in simulation at the top speed range of the flywheel units using the integrated model. In addition, experimental data was taken in the HEFF facility, with the flywheels operating between 8 and 20 kRPM (which represents the flywheels' extreme low speed operating range).

The results of each of the runs are presented, and comparisons are made between the simulations and experimental runs; these tests verify that the control algorithm is capable of controlling both the spacecraft bus and a single axis of attitude control. Also, the correspondence of the simulations and experiments demonstrates that the modeling of the subsystems was sufficient.

References

1. Panagiotis Tsiotras, Haijun Shen, Christopher Hall, "Satellite attitude control and power tracking with energy/momentum wheels," AIAA Journal of Guidance, Control and Dynamics, vol. 24, no. 1, pp. 23–24, 2001.
2. David Richie, Panagiotis Tsiotras, Jerry Fausz, "Simultaneous attitude control and energy storage using VSCMGs: theory and simulation," Proceedings of the American Control Conference, Arlington, VA, pp. 3973–3979, June 25–27, 2001.
3. Christopher Hall, "High speed flywheels for integrated energy storage and attitude control," Proceedings of the American Control Conference, Albuquerque, NM, pp. 1894–1898, June 1997.
4. Renuganth Varatharajoo, Stefanos Fasoulas, "Methodology for the development of combined energy and attitude control systems for satellites," Aerospace Science and Technology 6, vol. 6, no. 4, pp. 303–311, 2002.
5. Peter E. Kascak, Ralph Jansen, Barbara Kenny, Timothy Dever, "Single axis attitude control and DC bus regulation with two flywheels," NASA/TM—2002-211812, Proceedings of the 2002 Intersociety Energy Conversion Engineering Conference, Washington, D.C., July 28–Aug. 2, 2002.
6. Barbara H. Kenny, Ralph Jansen, Peter Kascak, Timothy Dever, Walter Santiago, "Demonstration of single axis combined attitude control and energy storage using two flywheels," IEEE Aerospace Conference, Big Sky, MT, March 6-13, 2004.
7. Larry Trase, "The evaluation and implementation of a water containment system to support aerospace flywheel testing," NASA/TM—2002-20023, Proceedings of the 2002 Intersociety Energy Conversion Engineering Conference, Washington, D.C., July 28–Aug. 2, 2002.
8. Meriam, Kraige, Engineering Mechanics Dynamics 2nd Edition, University of California Santa Barbara, CA, 1986.
9. R. Krishnan, Permanent Magnet Synchronous and Brushless DC Motor Drives: Theory, Operation, Performance, Modeling, Simulation, Analysis and Design, Virginia Tech., Blacksburg, Virginia, 1999.
10. Barbara H. Kenny, et al., "Advanced motor control test facility for NASA GRC flywheel energy storage system technology development unit," NASA/TM—2001-210986, Proceedings of the 2001 Intersociety Energy Conversion Engineering Conference, Savannah, Georgia, July 29–Aug. 2, 2001.

11. Barbara H. Kenny, Peter Kascak, "Sensorless control of permanent magnet machine for NASA flywheel technology development," NASA/TM—2002-211726, Proceedings of the 2002 Intersociety Energy Conversion Engineering Conference, Washington, D.C., July 28–Aug. 2, 2002.
12. Peter E. Kascak, Barbara Kenny, Timothy Dever, Walter Santiago, Ralph Jansen, "International space station bus regulation with NASA Glenn Research Center flywheel energy storage system development unit," NASA/TM—2001-211138, Proceedings of 2001 Intersociety Energy Conversion Engineering Conference, Savannah, Georgia, July 29–Aug. 2, 2001.
13. Barbara H. Kenny, Peter Kascak, "DC bus regulation with a flywheel energy storage system," NASA/TM—2002-211897, SAE Paper 02PSC-61, Proceedings of the SAE Power Systems Conference, Coral Springs, FL, Oct. 29–31, 2002.
14. Barbara H. Kenny, Peter Kascak, Ralph Jansen, Timothy Dever, "A flywheel energy storage system demonstration for space applications," NASA/TM—2003-212346, Proceedings of the International Electric Machines and Drives Conference, Madison, Wisconsin, June 1–4, 2003.
15. D.W. Novotny and T.A. Lipo, Vector Control and Dynamics of AC Drives, Oxford Science Publications, Oxford, 1996.

REPORT DOCUMENTATION PAGE

Form Approved
OMB No. 0704-0188

1. AGENCY USE ONLY (*Leave blank*)	2. REPORT DATE	3. REPORT TYPE AND DATES COVERED
	September 2005	Technical Memorandum

4. TITLE AND SUBTITLE

Demonstration of Attitude Control and Bus Regulation With Flywheels

5. FUNDING NUMBERS

WBS–22–612–50–81–11

6. AUTHOR(S)

Peter E Kascak, Ralph Jansen, Barbara Kenny, and Timothy Dever

7. PERFORMING ORGANIZATION NAME(S) AND ADDRESS(ES)

National Aeronautics and Space Administration
John H. Glenn Research Center at Lewis Field
Cleveland, Ohio 44135–3191

8. PERFORMING ORGANIZATION REPORT NUMBER

E–15237

9. SPONSORING/MONITORING AGENCY NAME(S) AND ADDRESS(ES)

National Aeronautics and Space Administration
Washington, DC 20546–0001

10. SPONSORING/MONITORING AGENCY REPORT NUMBER

NASA TM—2005-213867

11. SUPPLEMENTARY NOTES

Prepared for the 39th Annual Meeting sponsored by the Institute of Electrical and Electronics Engineers Industry Applications Society, Seattle, Washington, October 3–7, 2004 Peter E. Kascak and Ralph Jansen, University of Toledo, 2801 W. Bancroft Street, Toledo, Ohio 43606; Barbara Kenny, NASA Glenn Research Center; and Timothy Dever, QSS Group, Inc., 21000 Brookpark Road, Cleveland, Ohio 44135. Responsible person, Peter E. Kascak, organization code RPE, 216–433–8408.

12a. DISTRIBUTION/AVAILABILITY STATEMENT

Unclassified - Unlimited
Subject Categories: 20 and 44

Available electronically at http://gltrs.grc.nasa.gov

This publication is available from the NASA Center for AeroSpace Information, 301–621–0390.

12b. DISTRIBUTION CODE

13. ABSTRACT ***(Maximum 200 words)***

A flywheel energy storage device stores energy in a rotating mass. These devices can be used to perform the same function as traditional chemical batteries. In terms of the energy storage function, a flywheel system has significant advantages over chemical batteries: length of life, energy density, power density, and the capability of deep depth of discharge. Also, flywheels can be used to control the attitude of the spacecraft. This paper describes an experiment using two flywheels to simultaneously regulate a DC bus and provide single axis angle regulation on an air table. Models of the mechanical and electrical systems are developed, and simulations are run, then compared to experimental results. The correspondence of the simulations and experiments shows the sufficiency of the modeling of subsystems.

14. SUBJECT TERMS

Motor; Generator; Model; Flywheel; Attitude control; Energy storage

15. NUMBER OF PAGES

19

16. PRICE CODE

17. SECURITY CLASSIFICATION OF REPORT	18. SECURITY CLASSIFICATION OF THIS PAGE	19. SECURITY CLASSIFICATION OF ABSTRACT	20. LIMITATION OF ABSTRACT
Unclassified	Unclassified	Unclassified	